

# Velocity Probability Distribution Function in the Crossover and the Viscous Range

Jens Eggers<sup>1</sup> and Z. Jane Wang<sup>2†</sup>

(1) *Universität Gesamthochschule Essen, Fachbereich Physik, 45117 Essen, Germany*

(2) *Department of Theoretical Physics, University of Oxford, Oxford, OX1 3NP, UK*

(November 11, 2018)

## Abstract

We derive a multifractal model for the velocity probability density distribution function (PDF), which is valid from the inertial range to the viscous range. The model gives a continuous evolution of velocity PDFs from large to small scales. It also predicts the asymptotic form of the PDF of velocity gradients. More importantly, the model captures the crossover range behavior and thus allows us to address the transition observed in the Helium turbulence experiment [*Tabeling et. al., Phys. Rev. E53, 1613 (1996)*] quantitatively. We compare both the PDFs and the structure functions predicted by this model with the experiments from the inertial range to the smallest scale resolved by the experiment. The model also predicts that the flatness measured in the crossover region can decrease with the Reynolds number.

PACS numbers: 47.27.-i, 47.80.+v      *submitted to Physical Review E*

## I. INTRODUCTION

The statistics of a turbulent flow field can be characterized by a family of probability distribution functions (PDF) of velocity differences over varying spatial scales. At large scales, where the energy is fed into the system, the probability distribution is approximately Gaussian. As the scale decreases, the distribution develops increasingly stretched tails, which corresponds to large deviations from its average values, a phenomenon called intermittency. These intermittent fluctuations are believed to be a consequence of the nonlinear interactions between different scales. Through these nonlinear interactions the energy is transported from large to small scales. At each stage of the energy cascade, the velocity fluctuations are amplified. On a crude level, the cascade can be described by a random multiplicative process, which eventually is terminated by viscosity. At scales smaller than the viscous scale, the velocity field becomes smooth and its PDF reaches an asymptotic form. Previous studies have already examined the PDF of velocity gradients [1–3].

An equivalent description of the statistics of the velocity field is given by the structure functions  $D_q(r)$ :

$$D_q(r) = \langle u_r^q \rangle, \quad (1)$$

where  $u_r(x)$  is the velocity difference over  $r : [u(x+r) - u(x)]$ .

In the inertial range, where the details of the large scale flow and the viscosity are unimportant, the velocity distribution is self-similar in  $r$ . Consequently,  $D_q(r)$  is given by a power law:

$$D_q(r) = C_q(r/L)^{q/3+\delta\zeta_q}, \quad (2)$$

where the  $C_q$  are constants independent of  $r$  and the  $\delta\zeta_q$  are the so-called intermittency corrections to the scaling exponents. In the absence of intermittency, the scaling is described by the classical Kolmogorov 41 law [4]:

$$\delta\zeta_q = 0. \quad (3)$$

This corresponds to a case where the shape of the PDF does not depend on scale, and their variances decrease as  $r^{1/3}$ . In the viscous range,  $D_q(r)$  is simple because of the viscous smoothing:  $D_q(r) \sim r^q$ . On the other hand, the crossover region from the inertial range to the viscous range is far more complex. Nelkin [5] noted that because the local velocity is fluctuating in space, the viscous cutoff scale  $\eta_c$ , which depends on the local Reynolds number, must also be fluctuating in space. The local Reynolds number is defined as

$$Re_r = \frac{u_r r}{\nu}, \quad (4)$$

where  $\nu$  is viscosity. The fluctuations in  $\eta_c$  lead to an additional broadening of the velocity distributions. This effect can best be seen by considering a case in which the velocity distribution in the inertial range is Gaussian. Benzi et. al. [1] showed that the fluctuating  $\eta_c$  alone can lead to a stretched exponential distribution of the PDF of velocity gradients. In the presence of intermittency, these authors further derived a formula for the PDF of velocity gradients and of PDFs of velocity differences in the inertial range. We will generalize their results to include the crossover regime from the inertial range to the dissipation range, and we derive our results using continuous evolutions. A related work on comparing experiment data and multifractal model of PDFs can be found in reference [3]. Another parallel work by Frisch and Vergassola [6] studied the consequence of the fluctuating  $\eta_c$  in structure functions.

Our motivation to develop a model for PDFs of velocity differences over the full range of scales is threefold:

- (1) The PDFs are the experimentally measured quantities, and thus a model for the PDF allows for the most direct comparison with experimental data.
- (2) The crossover from inertial range to viscous range can be analyzed quantitatively.
- (3) The model allows us to go one step beyond the order of magnitude arguments generally made when comparing with the experiments. Once the adjustable parameters are fixed by comparing with one particular flow, parameters are known for all flows and predictions can be made and compared with the experiments.

Our model is particularly useful for analyzing a series of recent Helium turbulence experiments by Tabeling et al. [7], [8], [9]. We study in detail the quantitative comparison between the model and the experiments. We are particularly interested in the flatness because of the

reported transition seen in flatness at a Taylor Reynolds number of  $Re_\lambda \approx 700$ . Within our model, we find that the flatness is rapidly varying over a spatial scale between  $2\eta$  and  $20\eta$ . This means that measurements of the flatness are extremely sensitive to the experimental resolution, which lies in this range of scales. More interestingly, the ordering of the magnitude of the flatness as function of Reynolds number depends on the particular scale in the crossover range. This further suggests that the asymptotic value of the flatness can only be measured below  $\eta$ , where we find the PDF to reach its asymptotic form. We emphasize the important difference between the scale  $1\eta$  and  $10\eta$ , which is often indistinguishable in order of magnitude arguments like those made in reference [21].

In the next section we briefly describe the multifractal model of turbulence, and in Section 3 we generalize this idea to include viscous effects. The resulting model for PDFs is the central starting point of the paper. In Section 4 we determine the adjustable parameters of the model using the experimental data by Tabeling's group. In the subsequent section we discuss the evolution of the PDFs as a function of the separation evolving from the inertial to the viscous range. In Section 6 we compute the flatness as a function of scale and focus on its crossover behavior. In the final discussion, we review all points of agreement and the discrepancies between the experimental data and the multifractal model and relate our observation to the recently reported transition in the flatness.

## II. BASIC IDEA OF MULTIPLICATIVE PROCESSES IN TURBULENCE

Experimental studies have shown that the turbulence velocity field in the inertial range exhibit power law scaling as described in Eq. (2). All information on two-point correlations of the velocity field is contained in the spectrum of exponents  $\zeta_q$ . The scaling (2) can also be viewed as a consequence of a underlying multiplicative process, by which the energy is cascaded progressively from eddies of size  $r$  into eddies of size  $r/\lambda$ . The ratio of the velocities in successive steps is a stochastic variable  $s_i$ , whose statistics is determined by its probability distribution  $p_s(s_i)$ . The index  $i$  denotes the  $i$ th-step in the cascade from a given large scale  $L$  to  $r$ :

$$u_r = u_L \prod_{i=1}^n s_i. \quad (5)$$

Assuming that the  $s_i$  are identically distributed and uncorrelated, we then have for the velocity moments:

$$\langle u_r^q \rangle = \langle s^q \rangle^n \langle u_L^q \rangle, \quad n = -\log_\lambda \frac{r}{L}$$

and by comparison with (2)

$$\zeta_q = \frac{q}{3} + \delta\zeta_q = -\log_\lambda \langle s^q \rangle. \quad (6)$$

Since  $\zeta_3 = 1$  by the Kolmogorov structure equation, we have the constraint

$$\langle s^3 \rangle = 1/\lambda. \quad (7)$$

In the following we will be making the conventional choice  $\lambda = 2$ . In the context of our phenomenological description, this is of a little consequence. Using the known exponent spectrum  $\zeta_q$ , information on the distribution  $p_s(s)$  can be extracted through its moments. There have been attempts to measure  $p_s$  directly [13], but little is known about its shape theoretically. Technically it is convenient to approximate  $p_s$  by a bimodal distribution

$$p_s(s) = p\delta(s - s_1) + (1 - p)\delta(s - s_2). \quad (8)$$

Imposing (7) as a constraint, the two remaining parameters can be used to reproduce the first 18 moments to within experimental error [14]. One can imagine that many other parameterizations of  $p_s$  would work equally well.

Here we base our fit on the experimental exponents by Tabeling's group [9], which were obtained by using the method of extended self-similarity. We find

$$p = 0.688, \quad s_1 = 0.699, \quad s_2 = 0.947. \quad (9)$$

The predicted scaling exponents using the above parameters are compared with the experiments in the table below: The exponents agree with the established values obtained in various turbulence experiments [15,16] to within the error.

Given this simple model of a multiplier distribution, the PDF  $P_j(u)$  of velocity differences on level

$$j = -\log_2(r/L)$$

can be readily calculated: it is the distribution  $P_0(u)$  on the outer scale, convoluted with  $p_s$   $j$  times, giving

$$P_j(u) = \sum_{\kappa=0}^j \binom{j}{\kappa} \left(\frac{p_1}{s_1}\right)^{j-\kappa} \left(\frac{p_2}{s_2}\right)^{\kappa} P_0\left(\frac{u}{s_1^{j-\kappa} s_2^{\kappa}}\right). \quad (10)$$

An expression equivalent to (10), but using the random  $\beta$  model, was already given in [1]. Since  $r$  is a continuous variable, it is useful to generalize (10) to continuous values of  $j$ . This can be done using the Euler-McLaurin sum formula, which gives to lowest order

$$P_j(u) = \int_{\kappa}^j \binom{j}{\kappa} \left(\frac{p_1}{s_1}\right)^{j-\kappa} \left(\frac{p_2}{s_2}\right)^{\kappa} P_0\left(\frac{u}{s_1^{j-\kappa} s_2^{\kappa}}\right) d\kappa + \frac{1}{2} \left[ \left(\frac{p_1}{s_1}\right)^j P_0\left(\frac{u}{s_1^j}\right) + \left(\frac{p_2}{s_2}\right)^j P_0\left(\frac{u}{s_2^j}\right) \right]. \quad (11)$$

This proved to be an adequate approximation of (10) for integer values of  $j$  and smoothly interpolates in between. In the next section, we follow the above basic idea to model the inertial range scaling, and in addition we introduce a fluctuating cutoff to model the viscous effects.

### III. MODEL FOR THE PROBABILITY DISTRIBUTIONS OF VELOCITY DIFFERENCES

Our model of PDFs of velocity differences includes three basic elements: 1) the experimentally measured PDF of velocities at a large scale  $P_0$ , 2) the multiplier distribution  $p_s$ ,

and 3) the viscous cutoff mechanism. Once they are determined, we can compute the PDF of velocities for any given scale. Among the three elements,  $P_0$  is experimentally given, and  $p_s(s)$  is assumed to be of the form of Eq. (8), with three parameters given by Eq. (9). We then follow the Nelkin's idea [5] and introduce a viscous cutoff scale  $\eta_c$  at which the local Reynolds number is equal to a fixed value. The physical idea of this cutoff is that whenever the *local* Reynolds number of an eddy reaches a critical value  $Re_{cr}$ , it is smoothed out by viscosity and the cascade stops. Since one expects the structure of small-scale velocity fluctuations to be universal, the details of the cutoff mechanism will not depend on the specific flows, thus  $Re_{cr}$  should be universal. Furthermore, because the local Reynolds number  $|u_r|r/\nu$  is a fluctuating quantity, so is  $\eta_c$ . These fluctuations further modify the scaling in the dissipation range in addition to the inertial range fluctuations.

More specifically, we can construct the following ensemble for velocity differences  $u_r$ . For convenience, all quantities are assumed to be non-dimensionalized by the large scale  $L$  and the root-mean-squared velocity fluctuations on that scale

$$U_{rms} = [\langle u_L^2 \rangle]^{1/2}.$$

In computing the PDFs we treat the the positive and negative velocities independently. Here we only look at positive values of  $u_r$ , the negative values are treated separately, replacing  $u_r$  by its modulus. Letting  $r = 2^{-n}$ , each ensemble member is then constructed by the following procedure:

- (1) Choose a realization of the large scale velocity field  $u_0 \equiv u_L$ .
- (2) Multiply  $u_0$  with random multipliers  $s$  to obtain a realization on step  $j$  until either (a) level  $n$  is reached or (b) the condition  $u_j 2^{-j} \geq R$  is no longer satisfied. The constant  $R$  is simply  $R = Re_{cr}/Re$ . This cutoff level in a particular realization will be denoted by  $j_c$ .
- (3) In case (a)  $u_r = u_n$  is the desired value of  $u_r$ . If the cascade has stopped due to the action of viscosity on level  $j_c < n$ , the velocity difference over the distance  $2^{-j_c}$  is  $u_{j_c}$ . Therefore, on scale  $r$  we have  $u_r = u_{j_c} 2^{j_c - n}$ .

To derive probability distributions from this procedure, it is more convenient to treat the level number as a continuous variable. Accordingly, we will assume that the velocity distributions  $P_j$  on level  $j$  have been continued to all real values  $j$ , as we did in (11).

To find an explicit expression for the probability distribution of  $u_r$ , we need to find the relation between  $j_c$  and  $u_r$ . If  $u_0$  is already smaller than  $R$ ,  $j_c$  is equal to zero, and the corresponding  $u_r$  is  $u_0 2^{-n}$ . Thus  $j_c = 0$  for  $u_r \leq R 2^{-n}$ . If the cascade reaches step  $n$ ,  $u_n$  must have been larger than  $R 2^n$ , and thus  $j_c = n$  for  $u_r \geq R 2^n$ . In between, the cascade is terminated by viscosity. This means the cutoff condition  $u_{j_c} 2^{-j_c} = R$  must be satisfied, and thus  $u_r = R 2^{2j_c - n}$ . To summarize, we have

$$j_c = \begin{cases} 0 & \log_2 \frac{u_r}{R} \leq -n \\ n & \log_2 \frac{u_r}{R} \geq n \\ \frac{1}{2}(n + \log_2 \frac{u_r}{R}) & \text{elsewhere} \end{cases} \quad (12)$$

Physically, we expect the relation between  $j_c$  and  $u_r$  to be smooth, so we will be using a smoothed version of (12), given in Appendix A, which is one-to-one between  $j_c$  and  $u_r$  and has

the property  $j_c(u_r) \rightarrow 0$  for  $u_r \rightarrow 0$  and  $j_c(u_r) \rightarrow n$  for  $u_r \rightarrow \infty$ . The smoothing introduces an additional parameter  $\Delta$ , cf. (A1), which is the number of levels over which the cascade is gradually cut off. Thus the description of the viscous range introduces two parameters:  $Re_{cr}$ , which measures the relative importance of the viscous term, and  $\Delta$ , which measures the effectiveness of the viscous smoothing. In a small-scale regime of universal isotropic fluctuations, we expect both to be independent of the large-scale flow. Thus once they are adjusted, they can be applied to all other flows at different Reynolds numbers.

To compute the probability distribution  $P_r$  of  $u_r$ , we express the total probability of finding  $u_r$  between  $u_r(j_c)$  and  $u_r(j_c + \delta)$  through the densities  $P_j$ . Namely

$$\int_{u_r(j_c)}^{u_r(j_c+\delta)} P_r(u) du = \int_{u_{j_c}}^{\infty} P_{j_c}(u) du - \int_{u_{j_c+\delta}}^{\infty} P_{j_c+\delta}(u) du, \quad (13)$$

where  $u_{j_c}$  is the velocity on level  $j_c$ , which contributed to  $u_r$ . Hence  $u_{j_c} = u_r 2^{n-j_c}$ . The normalization condition (13) simply expresses the fact that contributions from levels between  $j_c$  and  $j_c + \delta$  correspond to the probability of cascading down at least to level  $j_c$ , minus the probability of even making it to level  $j_c + \delta$ . Letting  $\delta$  go to zero, we obtain

$$P_r(u_r) = \frac{\partial j_c}{\partial u_r} \left\{ \frac{\partial u_{j_c}}{\partial j_c} P_{j_c}(u_{j_c}) - \int_{u_{j_c}}^{\infty} \frac{\partial P}{\partial j} \Big|_{j=j_c} (u) du \right\}, \quad (14)$$

where  $j_c$  on the right hand side of (14) can be expressed through  $u_r$ . If  $r$  tends to zero, (14) gives the distribution of velocity gradients, for which the distribution was also derived in [1]. However, the approximation of [1] just corresponds to the first term in the curly brackets, while the second term was neglected. Note that (13) automatically ensures that  $P_r$  is normalized, since

$$\int_0^{\infty} P_r(u) du = \int_0^{\infty} P_0(u) du,$$

which means that  $P_r$  inherits its normalization from the top level distribution  $P_0$ . Thus (14), together with  $P_j(u)$  (cf. (11)) and  $j_c(u_r)$  gives an explicit formula for  $P_r(u_r)$ , which we implemented numerically. This is the central result of the paper, which will be explored in the sections below.

#### IV. COMPARISON WITH EXPERIMENT

We apply this model to a set of experimental data measured by Tabeling et. al. [7], [8], [9]. The experiment measures the longitudinal component of the turbulent velocity field inside a closed cylinder filled with Helium. The viscosity is varied by a technique similar to that used in the Rayleigh-Bernard system [17,18] to achieve a variation over 3 decades in Reynolds number. The measurements of various scaling laws are described in the above series of papers [7], [8], [9]. The Reynolds number dependence of the flatness is reported to have an abrupt change at the Taylor Reynolds number  $\approx 700$ : the flatness increases with the Reynolds number up to  $Re_\lambda \approx 700$  and then it decreases with the Reynolds number. However the origin of this transition has been subjected to much debate [19], [20], [21].

Because our model offers a comparison for the PDF, or equivalently for all structure functions, rather than just the scaling exponents, we can do a careful study to compare the model with the experiments and have a better understanding of the viscous scaling where the transition is seen. The PDF at the beginning of the cascade can be determined experimentally once we choose a sensible outer scale. Since the experiments were carried out in a fixed geometry, we expect that at a fixed outer scale, where the energy is fed in, the PDF of velocity differences is independent of the Reynolds number. We confirm this by analyzing the experimental data. By inspecting the scaling of the second order structure functions, we choose the outer scale to be  $L = 0.73cm$  for all flows. The scale is roughly 1/5 of the integral scale quoted in reference [7]. The reason we chose  $L$  to be somewhat smaller is that below  $L$  the scaling follows a power law, and boundary effects seem to be negligible. We then examine the PDFs of the normalized velocity differences over the separation  $L$ , and find that they collapse for all the flows as shown in Fig.1. The velocities are normalized by their variance  $U_{rms}$ . In the same plot, a Gaussian distribution is shown as a dot-dashed line for comparison. The PDF at the outer scale is already non-Gaussian because we have chosen  $L$  to be smaller than the integral scale of [7], for the reasons given above. Thus some growth of intermittent fluctuations has already taken place. Also the dynamics of the boundary layer may have an important effect, because the experiment is in a closed geometry. The small asymmetry of the PDF is consistent with the Kolmogorov structure equation, which gives a non-vanishing skewness of the velocity. By the construction of the model, the asymmetry will propagate down to smaller scales. The large scale velocity variances, which differ because of different driving, set the velocity scales at each cascade level. The ratio of the velocity variance and the rotational velocity at a fixed scale will be shown later. We emphasize that the collapse of the PDFs holds for Taylor Reynolds number ( $Re_\lambda$ ) ranging from 300 to 2000, which include both the flows below and above the reported transition at  $Re_\lambda \approx 700$ .

The collapse of the outer scale PDF  $P_0(u)$  implies the collapse of PDF in the inertial range at a fixed separation. To check this, we calculate the experimental PDF at a separation scale of  $L/4$ , and again we observe the collapse of the PDFs as shown in Fig.2.

We recall that Tabeling et. al. observed the collapse of the PDF in the inertial range only for sufficiently large Reynolds numbers [8]. However, as we show here, the collapse works equally well for small Reynolds number ( $Re_\lambda < 700$ , and correspondingly,  $Re < 10E4$ ) flows in the inertial range. We suspect the reason that the previous authors did not observe the same collapse for small Reynolds number flows is because they fixed a scale too small to be in the inertial range of the small Reynolds number flows.

Because the shape of the normalized outer scale PDF is constant at the energy-input scale, the corresponding velocity scale is uniquely determined by its variance  $U_{rms}(L)$ . It allows us to define a Reynolds number

$$Re = \frac{U_{rms}(L)L}{\nu}. \quad (15)$$

We remark that this definition is different from the one used previously [7]:

$$Re = \frac{\Omega R^2}{\nu}, \quad (16)$$

where  $\Omega$  is the rotation frequency and  $R$  is the radius of the apparatus. Equation (16) assumes that the velocity at the energy-input scale is proportional to  $\Omega R$ . We tabulate the

ratio of  $U_{rms}$  and  $\Omega R$  for different Reynolds numbers in Table 2 and find that they vary considerably. Many factors can contribute to these differences. Apart from the systematic errors in the measurements, the shear velocity profile depends on the Reynolds number. A better understanding of the instabilities of the driving flow and the dependence of the large-scale quantity  $\Omega R/U_{rms}(L)$  on viscosity is desirable. For our purposes, the Reynolds number defined in Equation (15) is adequate.

Another frequently used dimensionless quantity is the Taylor Reynolds number:

$$R_\lambda = \frac{U_{rms}\lambda}{\nu},$$

$$\lambda = \frac{U_{rms}}{\sqrt{(du/dx)^2}} = U_{rms}\sqrt{\frac{15\nu}{\epsilon}}, \quad (17)$$

where  $\epsilon$  is the average energy dissipation. The last identity assumes isotropy of the flows. Here  $\epsilon$  can be estimated by the large scale flow:

$$\epsilon = -\frac{4}{5}\frac{U_{rms}^3(L)}{L}. \quad (18)$$

In the subsequent discussions, we shall use the  $Re$  defined in Eq. (15), and the corresponding  $Re_\lambda$  can be found in Table (III) below.

The remaining two parameters are  $Re_{cr}$  and  $\Delta$  defined in the previous section. The critical Reynolds number  $Re_{cr}$  defines the threshold to be compared with the local Reynolds number  $Re_r$ . If  $Re_r < Re_{cr}$ , viscous diffusion dominates and the cascade stops. In real turbulence, the termination of the cascade is a gradual process. The gradual crossover is parameterized by  $\Delta$  in our model. One expects  $Re_{cr}$  and  $\Delta$  to characterize the viscous cutoff mechanism, independent of large scale flow. Ideally, one would like to choose one particular flow to fix  $Re_{cr}$  and  $\Delta$ , and use the same values for the rest of the flows studied. We remark that the constancy of  $Re_{cr}$  is an assumption of the multifractal theory of turbulence, which has not been checked explicitly before.

We now determine the values of  $Re_{cr}$  and  $\Delta$  using the flow with  $Re = 1.36E3$ . Starting from the PDF  $P_0$  of the velocity at the outer scale, we compute the evolution of the PDFs, and consequently the structure functions at smaller scales. The values of  $Re_{cr}$  and  $\Delta$  are adjusted such that the resulting  $D_2(r)$  agrees best with experiment. Because our algorithm allows for continuous evolution steps, we can compute a sufficient number of points along the  $D_2(r)$  curve necessary for a good comparison. We find

$$Re_{cr} = 85 \pm 3, \text{ and } \Delta = 0.4 \pm 0.1. \quad (19)$$

Figure 3 shows the comparison of the predicted  $D_2(r)$  and the experimental measurement. Because the crossover in  $D_2(r)$  is a sensitive function of  $Re_{cr}$ , this comparison gives a relative small fitting error, which is about 3%, as opposed to inspecting the overlap of the PDFs, which gives errors of about 15%.

We find that the predicted PDFs are insensitive to the values of  $\Delta$ , which is fixed to be 0.4 for all flows. To check whether  $Re_{cr}$  is indeed independent of Reynolds number, we repeat the above procedure for all the flows. The value of  $Re_{cr}$  is shown in the fourth column of Table III. It is evident that there are considerable fluctuations in  $Re_{cr}$ , which



correspond to about a factor of two in the value of the crossover scale between inertial and viscous range. In what follows we will use  $Re_{cr}$  as quoted in Table III for the individual runs, since otherwise the fits of the PDFs in the viscous range would be poor. Unfortunately, this means that there is an adjustable parameter for each run. We will bear this in mind when we compare the theory and the experiments. From the experimental data available to us, we are not able to pinpoint the reason for the deviations of  $Re_{cr}$  from a constant value. However, these fluctuations are at least consistent with the fluctuations seen in the energy dissipation [7,21].

Having determined all the adjustable parameters in the model, we can proceed to make predictions for various quantities of interest. Table III is a summary of the experimental and model parameters for the flows studied in this paper.

## V. EVOLUTION OF PDFS AND THEIR ASYMPTOTICS

In this section we show three results: 1) the model gives a correct description of the inertial range behavior, 2) it also captures the crossover from the inertial range to the dissipation range, and 3) the model gives an asymptotic probability distribution for the velocity derivatives, based upon which we compute the flatness. 1) and 2) have partly been seen in our previous discussion on  $D_2(r)$ . Here we look at them again in the PDF of the velocity differences.

We start from the PDF of velocity differences at the outer scale, and compute the subsequent PDFs as the scale decreases. We show the evolution of the PDFs for two typical flows: one below and one above the transition at the Reynolds number  $Re_\lambda \approx 700$ . Figure 4 shows the evolution of the PDFs for  $Re = 1.36E3$ , which corresponds to the Taylor Reynolds number  $Re_\lambda = 344$ , and Fig. 5 for  $Re = 1.17E4$  at  $Re_\lambda = 1626$ . The solid line represents the experimental measurement, while the diamonds show the theoretical prediction. Each series covers scales ranging from the outer scale to the smallest scale measured by the experiments.

Similar pictures are obtained for all the flows we study. As expected, the shape of the PDF evolves toward stretched-exponential curves. The stretched tails describe the increasingly frequent occurrences of large intermittent events. The distribution of the large events make significant contributions to higher moments. A typical measure of intermittency is the flatness, which will be the focus of the next section.

In the case of the smaller  $Re$  flow, theory and experiment agree down to the smallest scale resolved by the experiment. Both the experimental and the theoretical PDFs show no sign of reaching their asymptotics even at the smallest scales. In the case of the large  $Re$  flow, theory and experiment agree for a number of cascade steps, but eventually deviate as the scale decreases toward the limit of experimental resolution. While the theoretical PDF continues to evolve, the experimental PDF saturates. This saturation corresponds to a saturation in the flatness, as shown below.

We recall that the second order structure function  $D_2(r)$  agrees very well between theory and experiment at all scales and for both the smaller and the large Reynolds number flows. This however does not contradict the deviation we see in the PDF, which occur only in the tail of the distribution, because  $D_2(r)$  does not sensitively depend on the tail distribution.

To better understand the deviations in the PDF, we tabulate the scale  $L_c$ , where theory and experiment starts to deviate for all experimental runs in Table IV. At the smallest

Reynolds number there is agreement on all available scales, so  $L_c$  can only be bounded from above. For the other Reynolds numbers we have given the ratios  $L_c/L$  and  $L_c/\eta$ . The fact that  $L_c/L$  is constant for the higher Reynolds numbers indicates that there is a constant scale in the system. The other ratio  $L_c/\eta$ , on the other hand, does not offer a simple pattern.

We next use our model to follow up on the evolution of the PDFs below the smallest spatial resolution of the experiments. This should allow us to estimate whether experiments can reliably approximate the distribution of velocity derivatives. Figure 6 shows the theoretical PDFs at four different values of  $r/\eta$ . The largest,  $r/\eta = 19.3$ , is the separation where theory and experiment start to deviate. At half that separation, which is the smallest one measured experimentally, the theory predicts a much wider distribution. The theoretical distribution continues to evolve down to about half that scale, as shown by the distributions at  $r/\eta = 4.8$  and  $r/\eta = 2.4$ .

Thus the theoretical PDF reaches its asymptotics close to the Kolmogorov scale, typically at  $r \sim \eta$ . This then suggests that in order to understand the scaling of the velocity derivatives, the experiments need to resolve a smaller scale than they currently do, which is on the order of  $3\eta$  to  $10\eta$ , and is  $9.6\eta$  for this particular flow. On the basis of order of magnitude arguments, the difference between  $1\eta$  and  $10\eta$  is perhaps insignificant. However, we will show in the next section that the difference in the prefactor is crucial and is significant in interpreting the experimental measurements of the flatness.

## VI. FLATNESS

Once we have the PDF  $P(x)$  for the velocity difference in the asymptotic limit  $r \rightarrow 0$ , it is straightforward to compute the flatness:

$$F_0 = \frac{\int P(x)x^4 dx}{(\int P(x)x^2 dx)^2}. \quad (20)$$

It is also more revealing to plot the flatness  $F(r)$  as function of scale

$$F(r) = \frac{D_4(r)}{(D_2(r))^2}, \quad (21)$$

which for  $r \rightarrow 0$  coincides with the definition (20). This allows us to compare our model with the experiments. Figure 7 shows the theoretical prediction for  $F(r)$  for the Reynolds numbers studied, which is seen to saturate at a constant value  $F_0$ . This asymptotic value is consistent with a power law

$$F_0 \sim Re_\lambda^{0.15}. \quad (22)$$

The exponent agrees with the compilation of flatness by Van Atta et. al. [23]. The most important feature we observe in Fig. 7 is the pronounced crossover behavior, which depends on the Reynolds number. In particular, although in the true asymptotic limit the flatness increases with the Reynolds number, at a fixed scale in the crossover region the flatness decreases with the Reynolds number as clearly shown in this figure. Therefore, if experiments are limited to the resolution in the crossover region (which is typically  $3 - 10\eta$ ), it is

conceivable that the experiments can yield a result which shows a decrease of flatness with Reynolds number.

To understand the difference between theory and experiments in the crossover range in more detail, we plot  $F(r)$  for a single flow and also compare it with experimental measurements. In the theoretical curve, three distinct regions are seen. At large scales, which correspond to the inertial range,  $F(r)$  increases like  $r^{\zeta_4 - 2\zeta_2}$ . At about  $15\eta$  viscosity becomes effective and  $F(r)$  increases much more sharply, because of the additional fluctuations introduced by the fluctuating cutoff. But only at  $r \approx 1\eta$  does  $F(r)$  fully saturate, in agreement with our observations of the probability distribution. By comparison, the experimental results shows a relatively small viscous rise. Thus the experiments show only a small part of the viscous cutoff fluctuations predicted by theory.

One can further understand the width of the crossover range as a function of Reynolds number. The higher the viscosity, the earlier does the rise of  $F(r)$  set in. At the same time, the rise is sharper compared to the low viscosity flows, since the viscous cutoff fluctuates over a narrower range of scales [22]. The combined effect leads to a *reversal* in the magnitude of  $F$  at intermediate separations, the lowest Reynolds number leading to the largest value of the flatness, as we see in Fig. 7. This suggests strongly that one has to be extremely careful about comparing  $F$  at different Reynolds numbers if the spatial resolution is in the crossover range.

## VII. DISCUSSION

We have studied in detail a model of PDFs of turbulent velocity differences with the aim of understanding the crossover below the inertial range for two reasons: 1) the crossover range is far more complex and less understood than both the inertial range and the far dissipation range, and 2) we hope to gain some quantitative understanding of the behavior of flatness in the crossover range, which may shed some light on the recent controversy about the transition seen in the flatness [8].

In particular, we compare our model with the recent series of experiments by Tabeling's group. We find that in the small Reynolds number flows, the model and the experiments agree on the shape of PDFs down to the smallest scale resolved. On the other hand, in the large Reynolds number flows, the model shows departure from the experiment below a scale defined as  $L_c$ , which is on the order of  $10\eta$ .

We also observe that in the crossover range between  $2\eta$  and  $20\eta$  the model predicts that the flatness does not necessarily increase with Reynolds number. The flatness may also decrease as function of the Reynolds number at an intermediate scale. This results from a rapid growth of the flatness in the crossover regime, which is often neglected in the usual picture of the scale dependence of the flatness. Furthermore, the width of the crossover region does not simply scale a la Kolmogorov because of the fluctuations in the cutoff scale. Both effects are due to the viscous fluctuation in the crossover range. Thus the observed decrease of the flatness with Reynolds number in the crossover region can be interpreted as a signature of multifractality. We emphasize that it is crucial to take the crossover into account when interpreting the experiments, since most often the experiment resolution coincides with the crossover range.

There are some remaining puzzles. For example, we do not completely understand the fluctuations seen in the critical Reynolds number  $Re_{cr}$  defined for this model, nor do we understand why the flatness does not rise in the crossover range as sharply as predicted by the model. A better understanding of these issues requires further comparisons between this model and other experiments such as large closed geometry experiments or open flow experiments.

## ACKNOWLEDGMENTS

We thank L. Biferale, L. Kadanoff, D. Lohse, and P. Tabeling for useful discussions. We are indebted to Tabeling's group at Ecole Normale Supérieure for sharing their data with us. ZJW is grateful to the hospitality of Tabeling's group during her visits supported by the NATO grant under award number CRG-950245. She also acknowledges the support by the NSF-MRSEC Program at the University of Chicago and by the EPSRC grant through University of Oxford. JE is supported by the Deutsche Forschungsgemeinschaft through Sonderforschungsbereich 237.

† Current address: Courant Institute of Mathematical Sciences, New York University, 251 Mercer St., New York, NY 10012. Electronic mail: jwang@cims.nyu.edu.

## APPENDIX A: SMOOTHING

Here we briefly describe how a smooth function  $j_c(u_r)$  was obtained from (12). Putting  $\ell = \log_2 \frac{u_r}{R}$ , we first make sure that  $j_c = \frac{1}{2}(n + \ell)$  smoothly merges into  $j = n$  for  $\ell \approx n$ . A convenient parameterization is

$$\bar{j} = n + \frac{1}{2} \left[ \frac{\ell - n}{2} - \left( \Delta + \frac{(\ell - n)^2}{4} \right)^{1/2} \right]. \quad (\text{A1})$$

Here we introduced a parameter  $\Delta$ , which measures the width of the transition region. In Section 3 we compare with the viscous crossover of an experimentally measured structure function  $D_2(r)$  and find  $\Delta = 1$  to accurately describe experiments.

But  $\bar{j}$ , as defined by (A1) still goes to  $-\infty$  as  $u_r \rightarrow 0$ , while the lowest available level is 0. The approach of  $j = 0$  has to be fast enough to make  $\partial j_c / \partial u_r$  go to zero as  $u_r \rightarrow 0$ . Namely, in view of (14) this means that

$$P_r(u_r) \approx 2^n P_0(2^n u_r), \quad (\text{A2})$$

so one simply sees the gradient of the large scale fluctuations, as expected. This is achieved by putting

$$j_c = \frac{1}{4} \log_2(1 + 2^{4\bar{j}}). \quad (\text{A3})$$

We found that the details of the smoothing were inconsequential to the shape of the distribution as long as the basic properties of  $j_c(u_r)$  were satisfied. Thus (A1) and (A3) determine the function  $j_c(u_r)$  we will be using throughout this paper.

## REFERENCES

- [1] R. Benzi et. al., Phys. Rev. Lett. **67**, 2295 (1991)
- [2] L. Biferale, Phys. Fluids A **5**, 428 (1993)
- [3] P. Kailasnath, K. R. Sreenivasan, and G. Stolovitzky, Phys. Rev. Lett., **68**, 2766 (1992).
- [4] A. N. Kolmogorov, C. R. Dokl. Acad. Sci. URSS **30**, 301 (1941).
- [5] M. Nelkin, Phys. Rev. A **42**, 7226 (1992).
- [6] U. Frisch and M. Vergassola, Europhys. Let. **14**, 439, (1991).
- [7] G. Zocchi, P. Tabeling, J. Maurer, and H. Willaime, Phys. Rev. E **50**, 3693 (1994).
- [8] P. Tabeling *et al.*, Phys. Rev. E **53**, 1613 (1996).
- [9] F. Belin, P. Tabeling, and H. Willaime, Physica D **93**, 52 (1996).
- [10] A. N. Kolmogorov, J. Fluid Mech. **13**, 82 (1962).
- [11] B. B. Mandelbrot, J. Fluid Mech. **62**,331 (1974).
- [12] U. Frisch and G. Parisi, in: *Turbulence and predictability in geophysical fluid dynamics and climate dynamics*, edited by M. Ghil, R. Benzi, and G. Parisi, p.84 (North-Holland, Amsterdam-New York, 1985).
- [13] A. B. Chhabra and K. R. Sreenivasan, Phys. Rev. Lett. **68**, 2762 (1992).
- [14] J. Eggers and S. Grossmann, Phys. Rev. A **45**, 2360 (1992).
- [15] F. Anselmet, Y. Gagne, E. J. Hopfinger, and R. A. Antonia, J. Fluid Mech. **140**, 63 (1984).
- [16] B. Castaing, Y. Gagne, and E. J. Hopfinger, Physica D **46**, 177 (1990).
- [17] D. C. Threlfall, PhD. Thesis, Univ. of Oxford, 1976 (unpublished); J. Fluid. Mech., **67**, 1 (1975).
- [18] F. Heslot, B. Castaing, and A. Libchaber, Phys. Rev. A **36**, 5870 (1987).
- [19] F. Belin, P. Tabeling, and H. Willaime, J. de Physique, in press (1996).
- [20] K. R. Sreenivasan, unpublished.
- [21] V. Emsellem, L. P. Kadanoff, D. Lohse, P. Tabeling, Z. J. Wang, Phys. Rev. E. *in press* (1997)
- [22] J. Eggers and S. Grossmann, Phys. Lett. **153**, 12 (1991).
- [23] C. W. Van Atta and R. A. Antonia, Phys. Fluids **23**, 252 (1980).

TABLES

q	2	3	4	5	6	7	8	9	10
exp.	0.70	1.00	1.26	1.50	1.71	1.90	2.08	2.19	2.30
model	0.70	1.00	1.26	1.50	1.71	1.89	2.05	2.19	2.31

TABLE I. Inertial range scaling exponents  $\zeta_q$  of the velocity field. Compared are the experimental measurements and our fit Eqs. (8), (9).

$Re$	1.36E3	1.86E3	1.07E4	1.17E4	2.88E4
$\Omega R/U_{rms}(L)$	2.31	0.71	0.89	0.46	1.26

TABLE II. Comparison of our definition (15) of the Reynolds number, and the definition (16) of the experimental group for the different flows under consideration.

$Re$	$U_{rms}(L)(cm/s)$	$\nu(cm^2/s)$	$Re_{cr}$	$Re_\lambda$	$\eta(\mu m)$
1.360E3	34.93	1.88E-2	85.7	344.0	49.0
1.863E3	10.18	4.E-3	41.0	600.0	20.0
1.170E4	18.54	1.16E-3	58.5	1626.	5.9
1.073E4	20.52	1.4E-3	64.38	1802.	6.0
2.881E4	44.08	1.12E-3	115.2	2394.	4.1

TABLE III. Experimental parameters and fitted values of  $Re_{cr}$  for the experimental runs studied in this paper.

$Re$	$L_c/L$	$L_c/\eta$
1.360E3	$< 3E-2$	$< 4.5$
1.863E3	$2.2E-2$	8.1
1.073E4	$1.1E-2$	13.5
1.170E4	$1.1E-2$	13.8
2.881E4	$1.1E-2$	19.6

TABLE IV. The smallest scale  $L_c$  where the multifractal model still works.

## FIGURES

FIG. 1. PDF of the velocity difference at the outer scale  $L$  are plotted on a log-linear scale for all experimental runs under consideration. The velocity differences is normalized by its variance, and the PDF is normalized to unity.

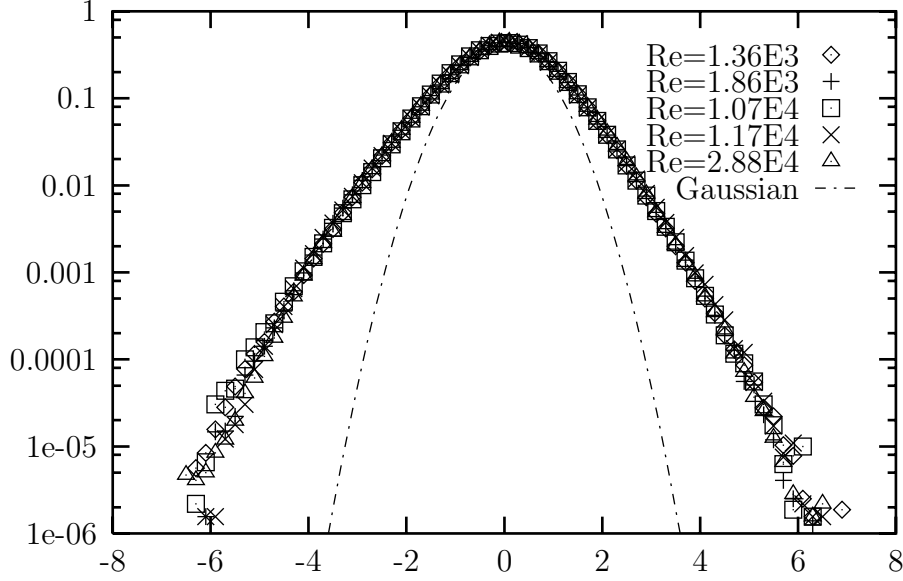


FIG. 2. PDF of the velocity difference at the scale  $L/4$  (still in the inertial range) for the same experimental runs as shown in Fig. 1. Again, the velocity difference is normalized by its variance, and the PDF is normalized to unity.

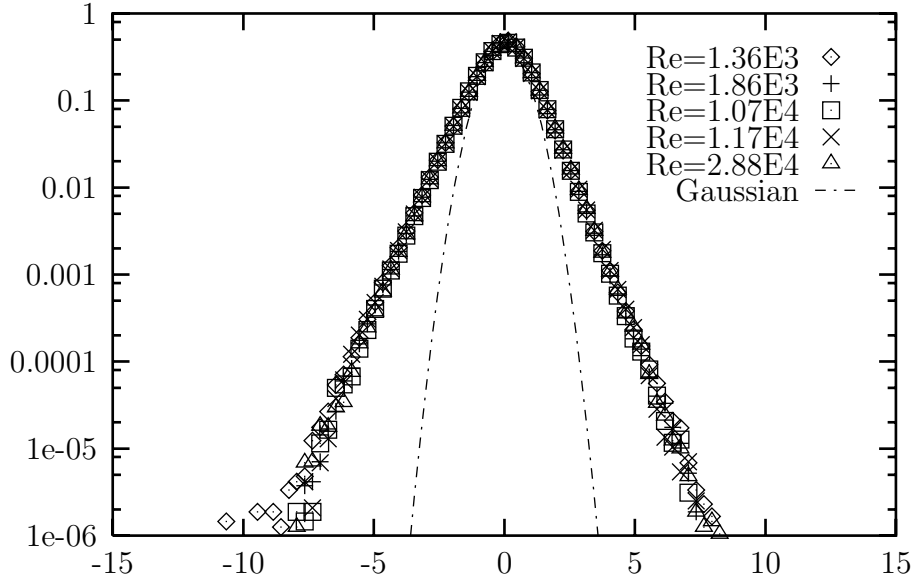


FIG. 3.  $\log D_2(r)$  plotted against  $\log(r)$  on a log-log scale. The separation  $r$  is normalized by the outer scale  $L$ .

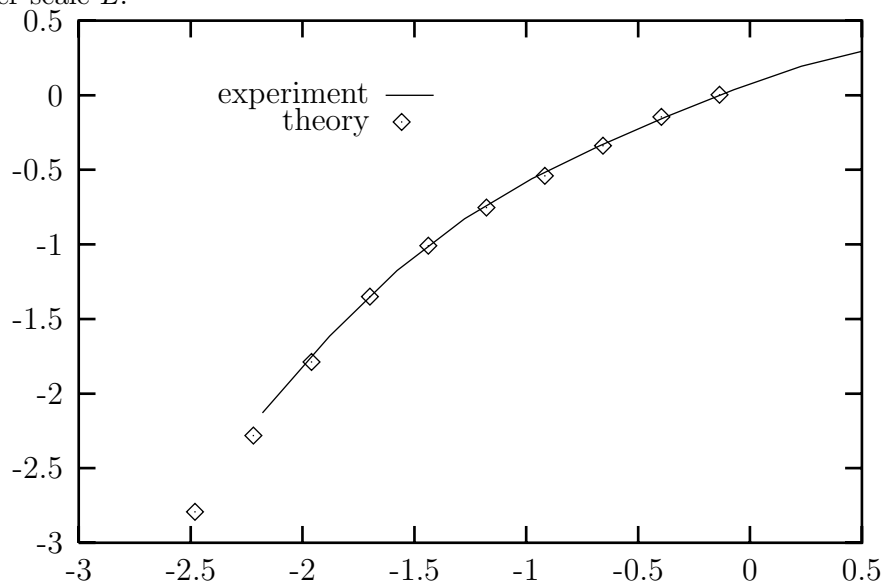
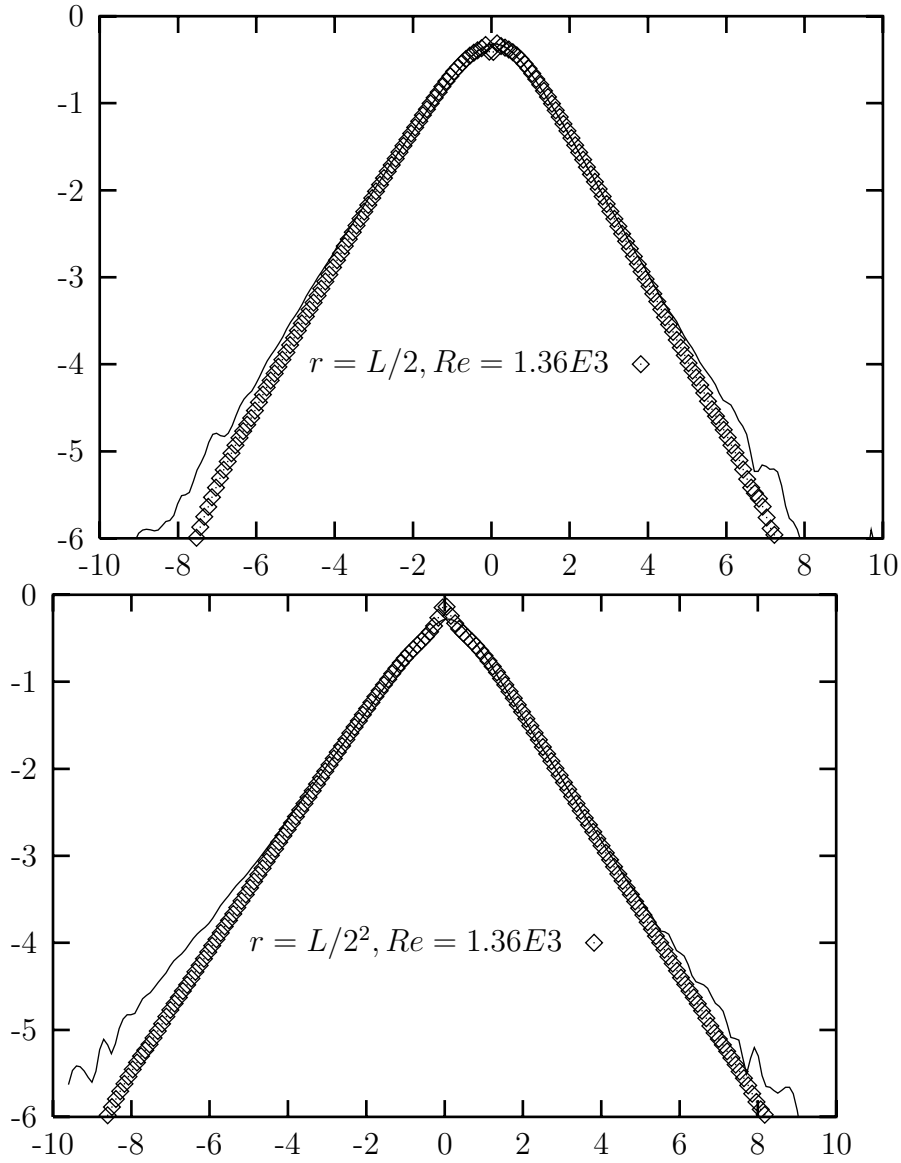




FIG. 4. Evolution of the logarithm of PDFs of velocity differences over different separations at  $Re = 1.36E3$ . The velocity difference is normalized by its variance, and the PDF is normalized to unity.



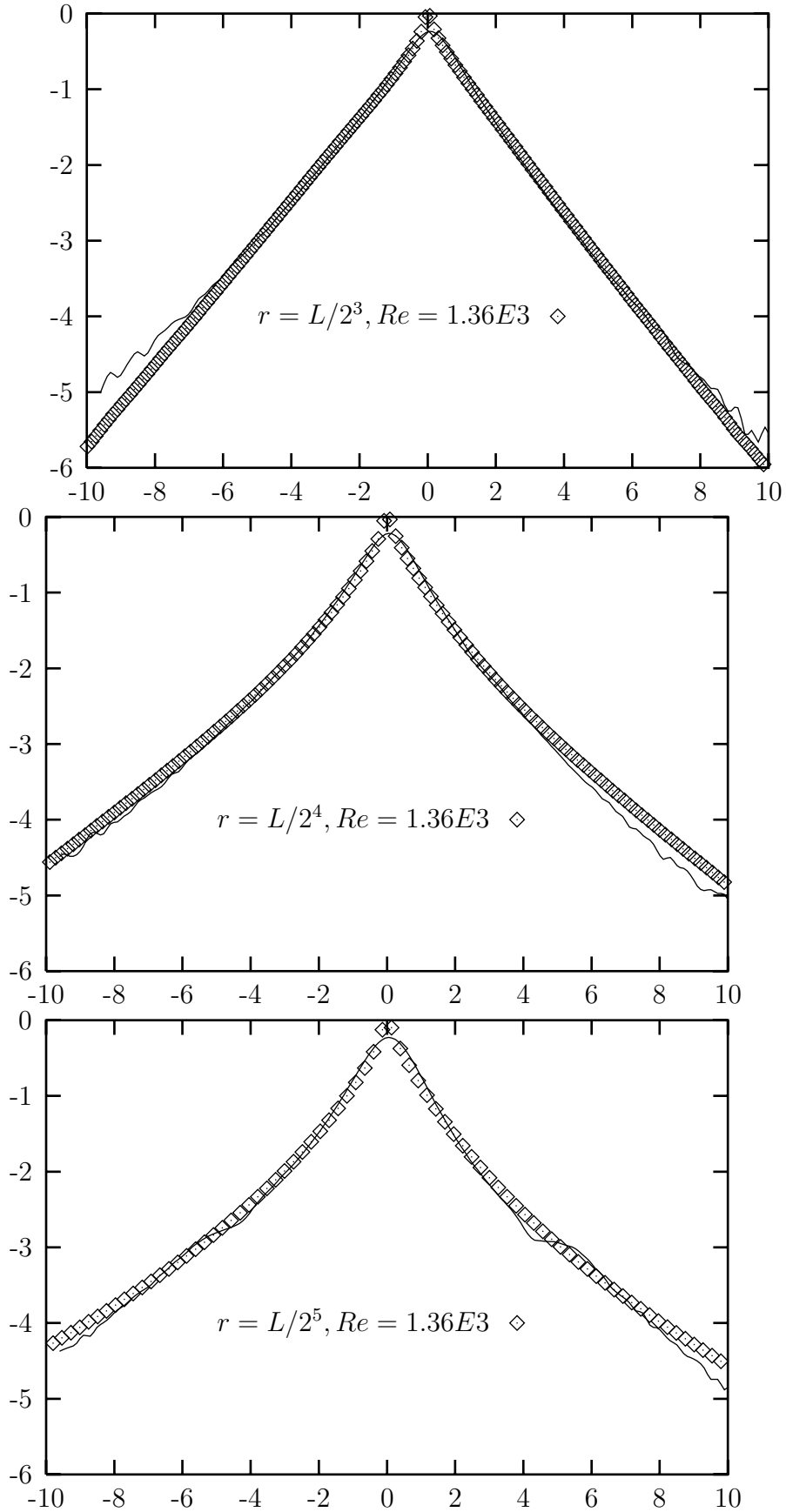
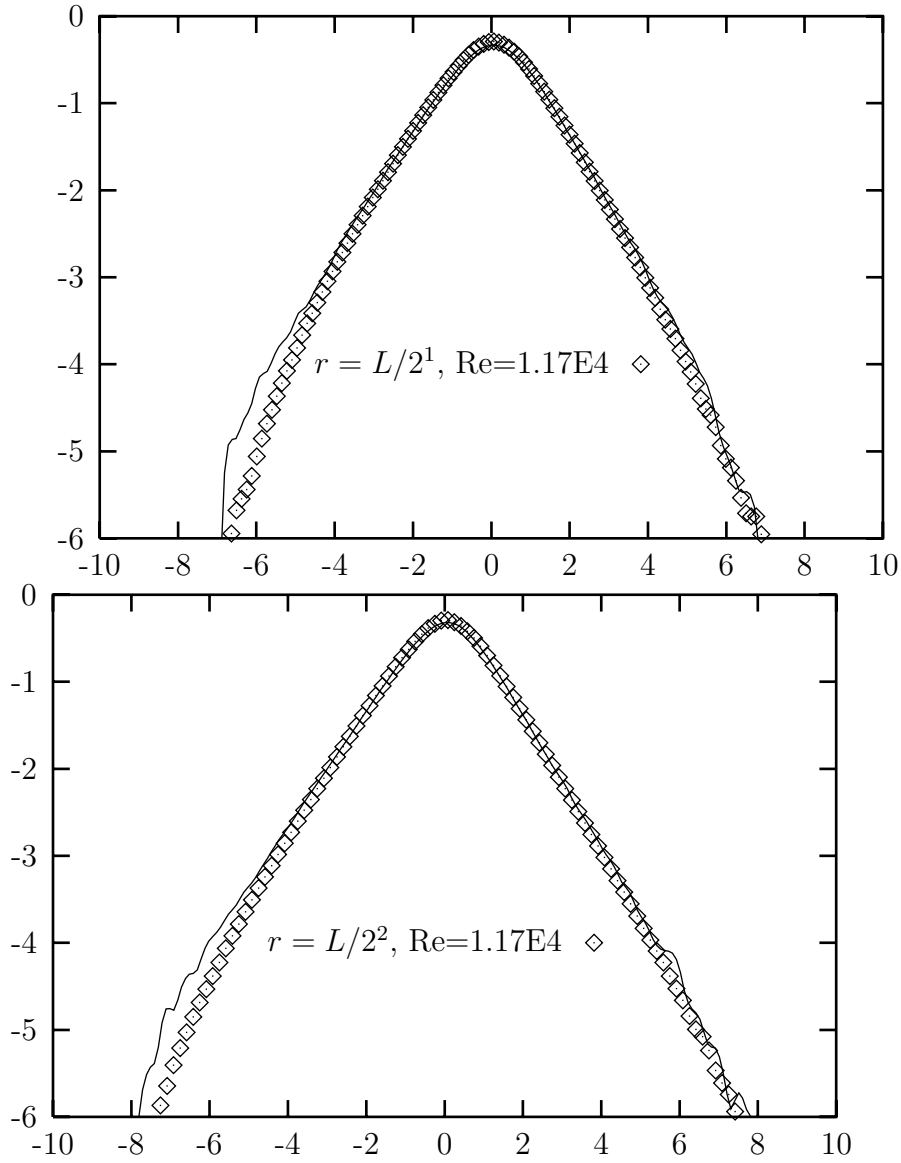
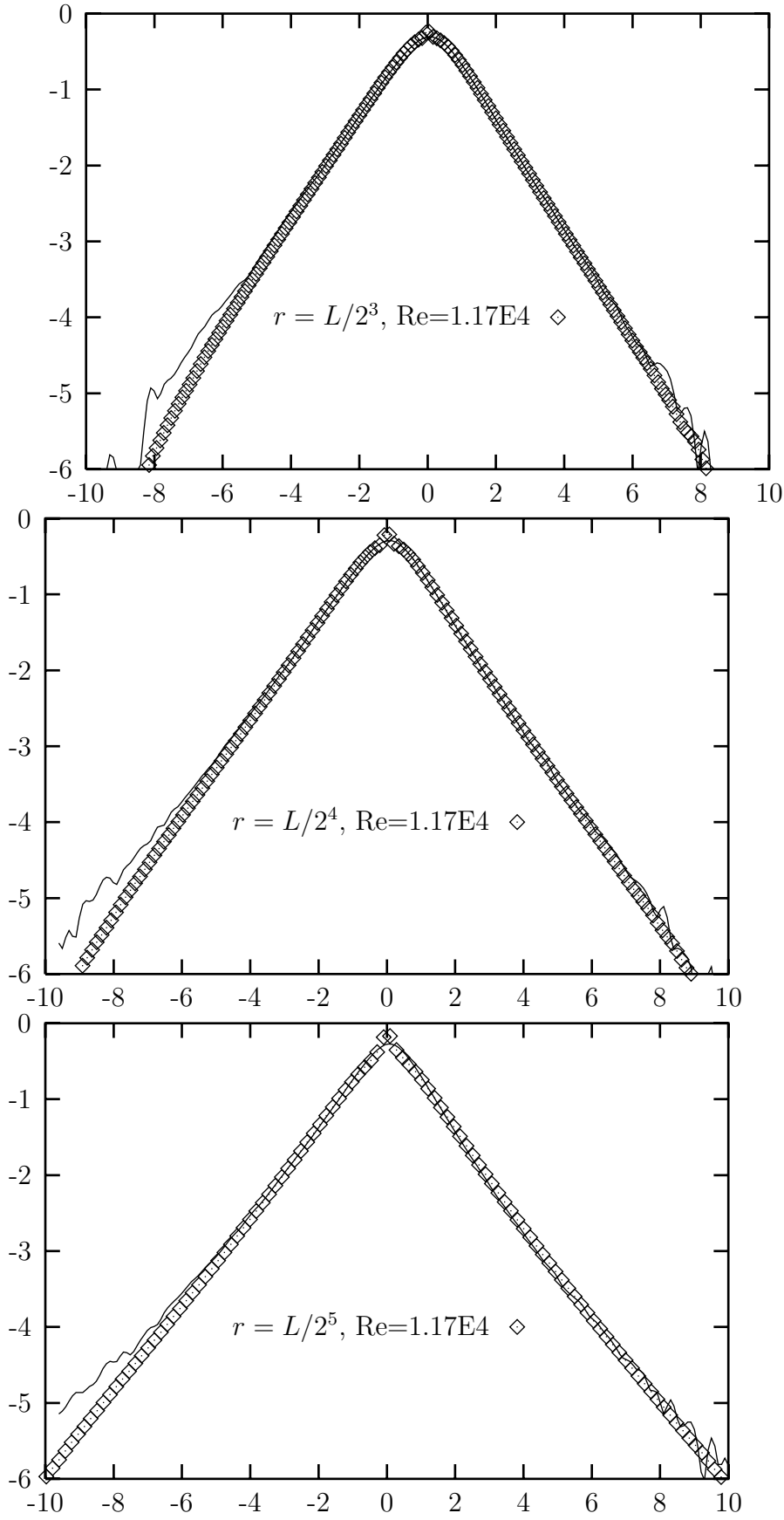


FIG. 5. Evolution of the logarithm of PDFs of velocity differences over different separations at  $Re = 1.17E4$ . The velocity difference is normalized by its variance, and the PDF is normalized to unity.





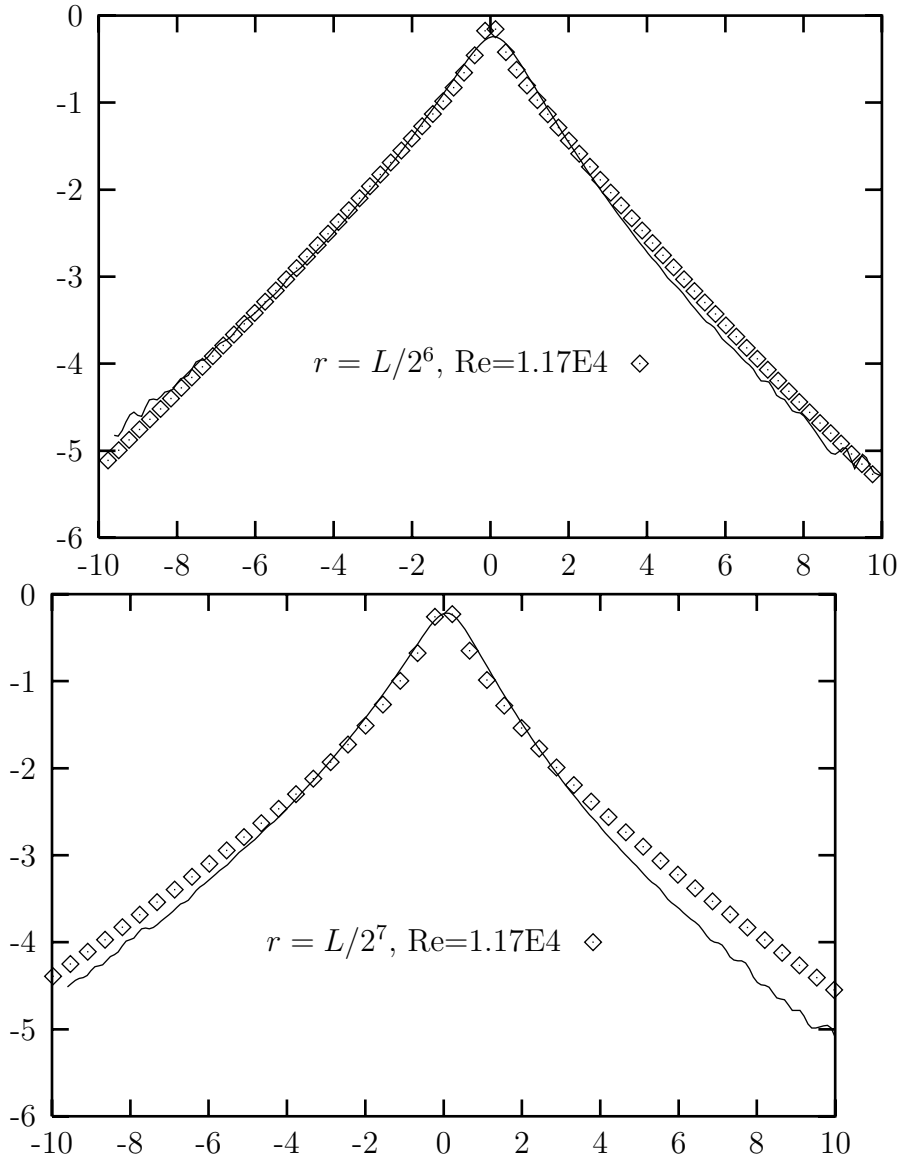


FIG. 6. A comparison of theoretical and experimental PDFs in the viscous range. The dashed line corresponds to the scale of experimental resolution. The last two curves show the asymptotic form of the PDF of the velocity gradients.

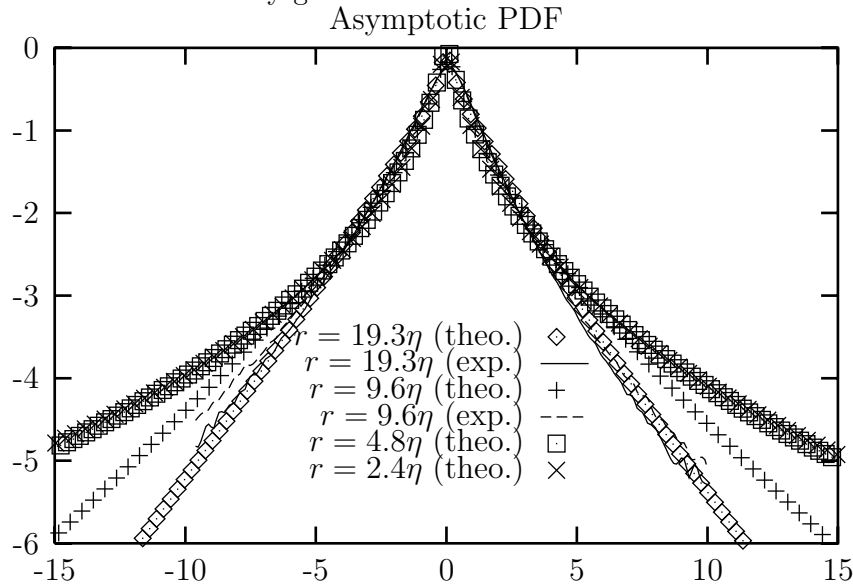


FIG. 7. The theoretical prediction for the scale-dependent flatness  $F(r)$  for different experimental runs. Note the sharp rise in the crossover regime, and the crossing of different curves in the same regime.

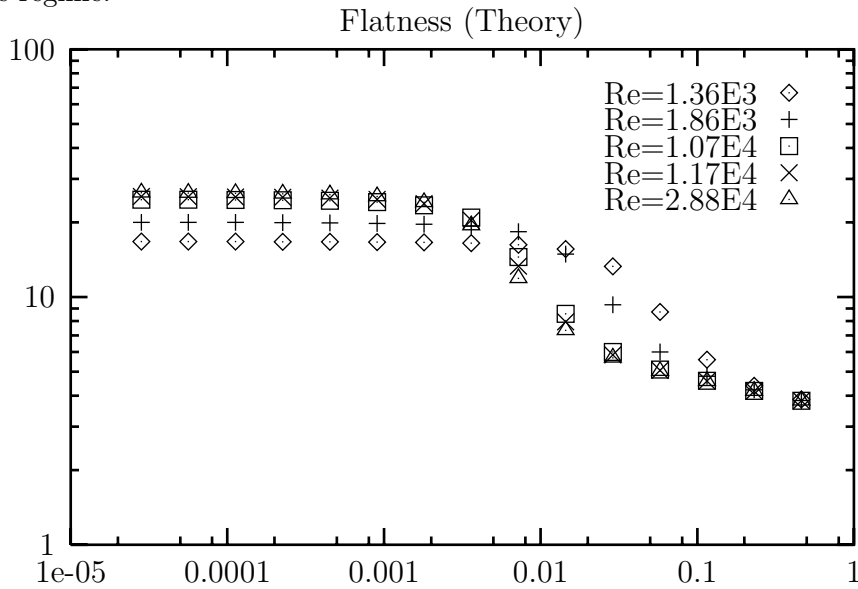


FIG. 8. A comparison of the experimental data for  $F(r)$  with the theoretical prediction for  $Re = 1.17E4$ .

